The oligomeric protein interference assay method for validation of antimalarial targets

de Assis Batista, Fernando

DOI:
10.33612/diss.94898872

4

STRUCTURAL ANALYSIS OF ASPARTATE TRANSCARBAMOYLASE FROM *Plasmodium falciparum* SUPPORTS ITS VALIDATION BY PROTEIN INTERFERENCE ASSAY

This chapter was adapted from: S. Lunev, S. S. Bosch, **F. A. Batista**, C. Wrenger and M. R. Groves. ***Crystal structure of truncated aspartate transcarbamoylase from Plasmodium falciparum.*** Acta Crystallographica Section F: Structural Biology Communications. 2016;72(Pt 7):523-33.

ABSTRACT

The de novo pyrimidine biosynthetic pathway of Plasmodium falciparum is a promising target for antimalarial drug discovery. The parasite requires a supply of pyrimidines for growth and proliferation and is unable to salvage the host pyrimidines. In the second step of plasmodial pyrimidine pathway, aspartate and carbamoyl phosphate are condensed to N-carbamyl-L-aspartate and inorganic phosphate via Aspartate transcarbamoylase (PfATC). In this chapter, a 2.5Å crystal structure of PfATC is reported. The PfATC model presented a high degree of homology with the catalytic domain of E. coli and similarly, it was modelled as a homotrimer where each of the three active sites is formed on the oligomeric interface. Each active site comprises the residues from two adjacent subunits in the trimer with a high degree of evolutionary conservation. Here, the activity loss due to mutagenesis of the key active site residues is also described.

4.1. INTRODUCTION

Plasmodial purine and pyrimidine metabolic pathways have been suggested as promising targets for anti-malarial drug research[1, 2] as they differ from those in host cells[3, 4]. *Plasmodium* parasites lack the *de novo* purine synthesis pathway and salvage the host cell purines for growth[5, 6]. Inhibition of this pathway was shown to be lethal for *P. falciparum*[7, 8]. Early biochemical studies on *P. berghei*[9–11], *P. Knowlesi*[12] and *P. lophurae*[13, 14] demonstrated the inability of *Plasmodium* species to metabolize pyrimidines. The parasites lack the thymidine kinase, an enzyme responsible for salvaging host thymidine, as confirmed by the completion of the *Plasmodium* genome sequence[15]. Therefore, parasites from the genus *Plasmodium* do not possess active pyrimidine salvage pathways and depends entirely on *de novo* synthesis through a series of enzymatic reactions. Plasmodial pyrimidine biosynthesis is also affected, directly or indirectly, by many of the current antimalarials[16]. For example, one of the most used current antimalarial drugs, Atovaquone[17], is known to inhibit cytochrome b in complex III of the respiratory chain and thus collapse the mitochondrial intra-membrane potential. This inhibition causes failure to provide oxidized ubiquinone to the fourth enzyme in the pyrimidine biosynthetic pathway, Dihydroorotate dehydrogenase (*Pf*DHODH)[18, 19], which was validated as an essential enzyme for the parasite and thus, a promising drug target[16, 20, 21].

This chapter is focused on another component of the plasmodial pyrimidine biosynthetic pathway, the enzyme aspartate transcarbamoylase. This enzyme catalyses the second step of the pyrimidine biosynthesis, the condensation of aspartate and carbamoyl phosphate to form N-carbamoyl-L-aspartate and inorganic phosphate. Here we report the crystal structure and preliminary characterization of truncated *Pf*ATC. Structural information was used to design the mutant version of *Pf*ATC with significantly reduced catalytic activity. The activity profiles of the mutants, as well as the wild-type enzyme, are reported. These data represent a next step in understanding the role of plasmodial aspartate metabolism and pyrimidine biosynthesis and support for the validation of *Pf*ATC as a drug target by the use of protein interference assay.

4.2. MATERIALS AND METHODS

4.2.1. CLONING

A full-length gene encoding for *Pf*ATC was amplified via reverse transcriptase PCR using *P. falciparum* total RNA as a template. In the first step, the cDNA was synthesised from RNA using Maxima First Strand cDNA Synthesis Kit for RT-qPCR (Thermo Scientific). In the second step, the full-length *Pf*ATC gene was amplified from the cDNA template using sequence-specific oligonucleotides (table 4.1). The PCR reaction was performed using SuperMix HiFi polymerase mix (Invitrogen). The generated PCR product was digested with BsaI and cloned into a pASK-IBA3 vector (IBA Lifesciences) previously digested with the same enzyme. The final expression plasmid pASK-IBA3-*Pf*ATC-full encoded the full-length version of *Pf*ATC with the additional amino acids SAWSHPQFEK (Strep-tag) at the C-terminus. Cloning of the truncated *Pf*ATC (for convenience the truncated *Pf*ATC-Met3 will be further referred as *Pf*ATC) was performed via PCR amplification using pASK-IBA3-*Pf*ATC-full plasmid as a template and sequence-specific oligonucleotides (table 4.1). The PCR fragment was similarly cloned into pASK-IBA3 vector previously digested with BsaI. The final expression plasmid pASK-IBA3-*Pf*ATC encoded the truncated version of *Pf*ATC (residues 37-375) with the additional amino acids SAWSHPQFEK (Strep-tag) at the C-terminus. All plasmid samples were verified by automated sequencing (Sanger).

Table 4.1 | Primer sequences used in the study. The recognition sites for restriction enzymes (specified in the primer name) are highlighted in bold. Mutations sites are underlined.

Primer	Sequence
*Pf*ATC-full cloning for recombinant expression (pASK-IBA3, strep-tag)	
IBA3-ATCfull-s (BsaI, Strep)	5´-GCGCGC**GGTCTC**CAATGATTGAAATATTTTGCACTGC-3´
IBA3-ATCfull-as (BsaI, Strep)	5´-GCGCGC**GGTCTC**CGCGCTGCTAGTTGATGAAAAAATGAG-3´
*Pf*ATC-met3 sub-cloning for recombinant expression (pASK-IBA3, strep-tag)	
IBA3-ATC-s (BsaI, Strep)	5´-GCGCGC**GGTCTC**CAATGTTTTATATCAATAGCAAG-3´
IBA3-ATC-as (BsaI, Strep)	5´-GCGCGC**GGTCTC**CGCGCTGCTAGTTGATGAAAAAATGAG-3´
*Pf*ATC-R109A/K138A Site-directed mutagenesis primers	
ATC-R109A-s	5´-GTTCCTTGAACCAAGTACAGCAACAAGATGTTCTTTTGATGC-3´
ATC-R109A-as	5´-GCATCAAAAGAACATCTTGTTGCTGTACTTGGTTCAAGGAAC-3´
ATC-K138A-s	5´-CTGATATGAATTCAACTTCTTTTTATGCGGGAGAAACTGTTGAAGATGCC-3´
ATC-K138A-as	5´-GGCATCTTCAACAGTTTCTCCCGCATAAAAAGAAGTTGAATTCA TATCAG-3´

4.2.2. PROTEIN EXPRESSION AND PURIFICATION

*Pf*ATC (truncated) was recombinantly expressed using *E. coli* Rosetta 2 (DE3) pLysS (Nalgene) competent cells transformed with pASK-IBA3-*Pf*ATC expression plasmid. The culture was propagated in 1 L of selective LB media supplemented with 50 μg ml^{-1} ampicillin, 35 μg ml^{-1} chloramphenicol and 4 mM $MgCl_2$ at 37°C and induced with 60 ng ml^{-1} of Anhydrotetracycline (AHT). The temperature of the culture was lowered to 18°C after induction and cells were harvested by centrifugation after overnight expression. Purification of recombinant *Pf*ATC was performed via Strep-Tactin chromatography according to the manufacturer's recommendations (IBA Lifesciences). The bacterial pellet from 1 L culture was resuspended in 40 ml Lysis buffer [50 mM Tris-HCl pH 8.0, 300 mM NaCl, 5% (v/v) glycerol, 3 mM β-mercaptoethanol (BME)]. The lysis was performed by sonication on ice. The supernatant containing soluble STREP-tagged *Pf*ATC was clarified by centrifugation. The soluble fraction was incubated with 2.0 ml Strep affinity resin (Strep Tactin Superflow, IBA Lifesciences) for 20 minutes at 4°C and subsequently collected with gravity-flow column (BioRad) and washed with 100 ml Lysis Buffer. The protein was eluted with 8 ml Elution buffer [50 mM Tris pH 8.0, 300 mM NaCl, 2.5 mM desthiobiotin, 5% (v/v) glycerol, 3 mM BME]. The eluate was pooled and concentrated at 4°C to 2 mg ml^{-1} using Vivaspin 4 concentration column with a 10 kDa cut-off (Sartorius Stedim Biotech).

In order to select the correct buffer for further purification Thermofluor-based stability assay was performed[22, 23]. Thermofluor data was collected using a CFX96 Real-Time system (Bio-Rad). SYPRO Orange dye (5000x stock, Invitrogen) was added to the protein sample (2 mg ml^{-1}) at 1:500 ratio. Each experiment consisted of 5 μl of the protein/dye mixture and 45 μl of the buffer component to be screened. Water was used as a control instead of the buffer sample. Inflexion points in graphs of relative fluorescence units (RFU) against temperature were determined manually and used as an indicator of the sample thermal stability in the presence of the screened buffer components. Components that exhibited a positive thermal shift in comparison to a water control sample were selected for gel-filtration buffer composition. The remaining eluate was concentrated to a volume of 1 ml (Vivaspin4, Sartorius Stedim Biotech) and purified via size-exclusion chromatography using HiLoad 16/60 Superdex 75 column (GE Healthcare) pre-equilibrated with Gel-filtration buffer [20 mM Tris pH 8.0, 300 mM NaCl, 10 mM Na-Malonate, 5% (v/v) glycerol and 2 mM BME]. The purified protein eluted as a single peak and was pooled and concentrated to 10 mg ml^{-1} at 4°C. The final concentration was determined based on the proteins theoretical absorbance at 280 nm [Abs 0.1% (1 mg ml^{-1})=0.84; http://web.expasy.org/protparam]. The concentrated protein was immediately used in crystallisation trials. The estimated protein purity was higher than 95% assessed by

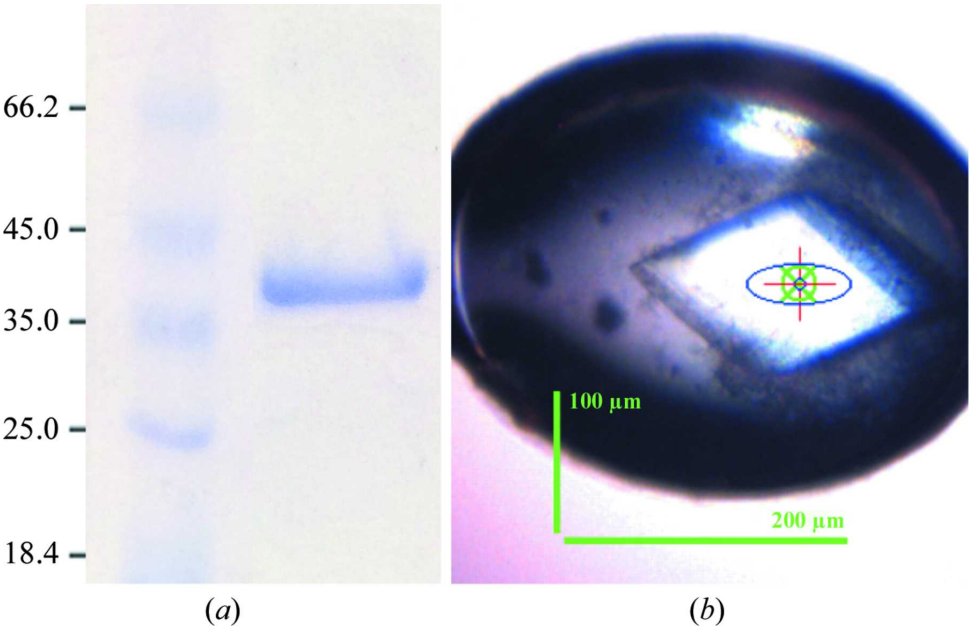

Figure 4.1 | (a) 10% SDS–PAGE of the purified *Pf*ATC. Sample was boiled in SDS-loading buffer prior to loading and the gel was stained with Coomassie Blue. Left lane - unstained protein marker (Thermo Scientific; labelled in kDa), right lane – *Pf*ATC sample. (b) Mounted in a cryo-loop (Molecular Dimensions) diffraction-quality single *Pf*ATC crystal grown in 200 mM Sodium sulphate, 5 mM $MgSO_4$, 15-18% (w/v) PEG 3350 in 100 mM bis-Tris Propane pH 7.5.

Coomassie Brilliant Blue-stained SDS-PAGE[24](Figure 4.1a). Expression and purification of the mutant version of *Pf*ATC were performed identically.

4.2.3. CRYSTALLISATION, X-RAY DATA COLLECTION AND STRUCTURE DETERMINATION

Screening for crystallisation conditions for *Pf*ATC was performed using High-throughput crystallisation robot (Gryphon, Art Robbins) against commercially available sparse-matrix screening kits (JCSG plus and PACT premier; Molecular Dimensions). All experiments were performed at 20°C using sitting drop vapour diffusion technique in 96-well MRC plates (Molecular Dimensions). Equal volumes (0.1 µL) of protein solution and crystallisation reagent were equilibrated against 50 µL of reservoir solution. Medium-size single crystals appeared overnight in various conditions containing PEG 3350/4000. Further optimization was performed by varying the precipitant concentration, ionic strength, the pH and the buffer type. The optimal conditions consisted of equal amounts (1.5 µl) of 9

mg ml^{-1} *Pf*ATC sample and 0.2 M Sodium Sulphate, 5 mM $MgSO_4$, 15-18% (w/v) PEG 3350 in 0.1 M bis-Tris Propane pH 7.5 as the crystallisation solution at 20°C. The rhomboid-shaped diffraction-quality crystals (Figure 4.1b) with maximum dimensions of 200µm appeared overnight and were subsequently harvested using mounted round Lytholoops (Molecular Dimensions), incubated in the Cryo-buffer and flash-frozen in liquid nitrogen prior shipment to the synchrotron. The Cryo-buffer was chosen based on the estimation from (Garman and Mitchell 1996) and consisted of 0.2 M Sodium Sulphate, 5 mM $MgCl_2$, 15-18% (w/v) PEG 3350, 20% glycerol in 0.1 M bis-Tris Propane pH 7.5. Cryocooled *Pf*ATC crystals were sent to the European Synchrotron Radiation Facility (ESRF), Grenoble using a dry-shipping cryo-container and a 2.4Å resolution data set was collected at -173°C in a nitrogen stream on the ID23-2 beamline (Figure 4.2). Initial characterization of the crystals and the optimization of data-collection parameters were performed using BEST[25]. The space group of the *Pf*ATC crystals was calculated to be monoclinic $P2_1$, with unit-cell parameters a=87.0, b=103.8, c=87.1Å, α=90.0, β=117.7, γ=90.0°, and the solvent content was calculated to be 59.4%. The data were processed using XDSAPP[26]. The analysis also showed that the crystals were twinned. The Matthews coefficient[27] predicted that the asymmetric unit is likely to contain three monomers of *Pf*ATC. The data collection and processing statistics are reported in Table 4.2.

The structure of *Pf*ATC was solved by molecular replacement using BALBES software[28] within the CCP4 package[29]. The X-ray structure of ATC from *Pyrococcus abyssi*[30] was used as a search model yielding a solution of three molecules in the asymmetric unit. The model was further optimized using manual rebuilding via COOT[31] and refined with REFMAC software[32]. The final refinement steps were carried out with global NCS restraints and TLS restraints calculated via TLSMD web server[33, 34]. The final 2.5Å model of *Pf*ATC consisted of 3 molecules in the asymmetric unit with R-factor of 0.215 and a free R-factor of 0.259 (Table 4.2) and was deposited in the Protein Database (PDB) with accession code 5ILQ. The structure figures were prepared with PyMol[35].

4.2.4. MUTAGENESIS

The double mutant *Pf*ATC-R109A/K138A was created via site-directed mutagenesis using specific oligonucleotides (Table 4.1) and the previously described pASK-IBA3-*Pf*ATC expression plasmid as a template. The PCR reaction was performed using Phusion Hot Start II DNA polymerase (Thermo Scientific) according to the manufacturer's recommendations. The generated mutant plasmid was treated with DpnI for 2 hours at 37°C to eliminate the parental template. The resulting double mutated plasmid (pASK-IBA3- *Pf*ATC-R109A/K138A) encoded for the truncated *Pf*ATC with corresponding point

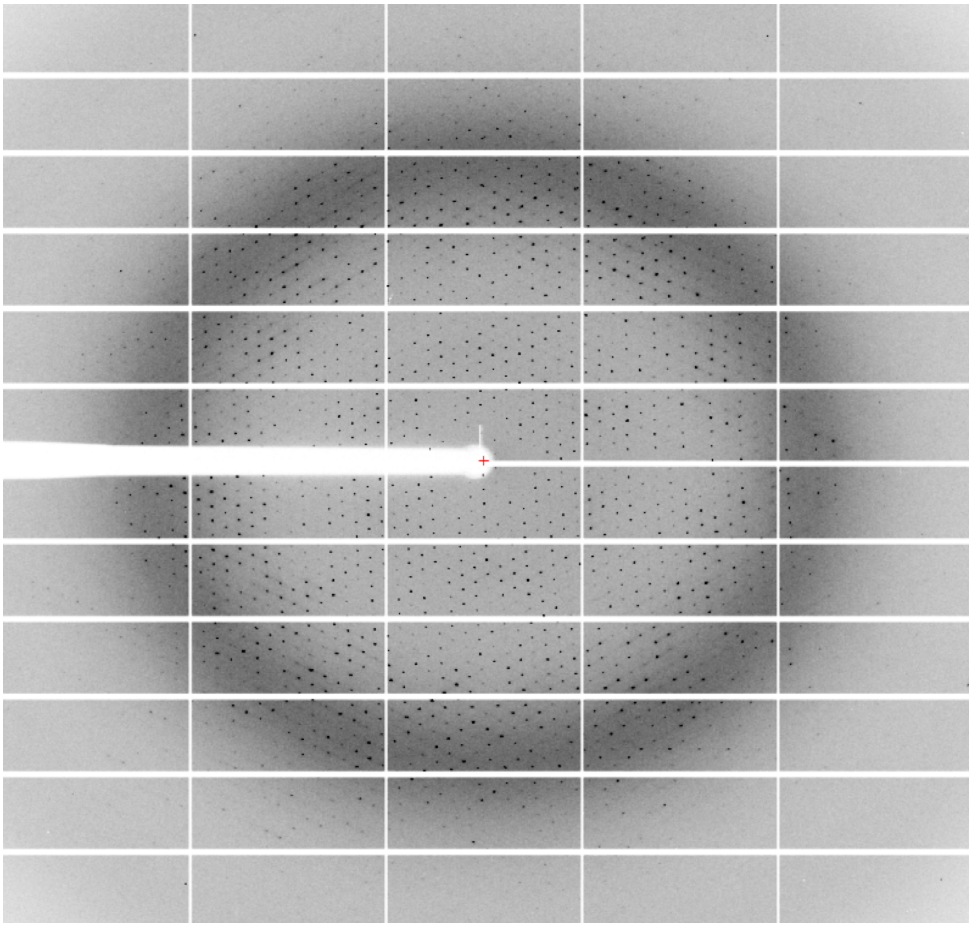

Figure 4.2 | Example of the diffraction frame obtained from a *Pf*ATC crystal on beamline ID23-2 at ESRF, Grenoble. The corresponding beamline parameters are given in Table 4.2

Table 4.2 | Data collection and refinement statistics of *Pf*ATC. Values for the outer shell are given in parentheses.

Data collection	
Diffraction source	ESRF ID 23-2
Wavelength (Å)	0.98
Detector	PILATUS 6M
Crystal-detector distance (mm)	337.55
Rotation range per image (°)	0.1
Total rotation range (°)	129
Exposure time per image (s)	0.04
Space group	$P2_1$
a, b, c (Å)	86.96,103.80,87.11
α, β, γ (°)	90.0,117.69,90.0
Mosaicity (°)	0.2
Resolution range (Å)	45.0 – 2.42 (2.56 – 2.42)
Total No. of reflections	126651 (20324)
No. of unique reflections	50423 (8051)
Completeness (%)	95.9 (95.6)
Redundancy	2.51 (2.52)
$<I/\sigma(I)>$	10.81 (1.98)
R_{meas} (%)	7.6 (58.0)
Overall B factor from Wilson plot (Å^2)	56.64
Refinement	
Resolution range (Å)	20.0 – 2.5
Completeness (%)	95.15
σ cutoff	1
No. of reflections, working set	42863
No. of reflections, test set	2354
Final R_{cryst}	0.18
Final R_{free}	0.22
Cruickshank DPI	0.2743
No. of non-H atoms	7909
Protein	7801
Ion	23
Water	88
R.m.s. deviations	
Bonds (Å)	0.019
Angles (°)	1.96
Average B factors (Å^2)	57.39
Protein	58.04
Ion	56.76
Water	51.47
Ramachandean plot	
Most favoured (%)	93.60
Allowed (%)	5.98

mutations and a C-terminal STREP-tag. The mutations were validated by sequencing (Sanger).

4.2.5. ACTIVITY ASSAYS

The kinetic properties of *Pf*ATC, as well as its mutant version *Pf*ATC-R109A/K138A, were investigated according to[36] and [37] with minor modification. Briefly, the reaction was carried out at room temperature in a total volume of 160µl of 14 mM L-aspartate and 1 mM carbamoyl phosphate (CP) substrate solution in 200mM Tris-Acetate buffer pH 8. The reaction was stopped by 80 µl of 25 mM ammonium molybdate in 4.5 M H_2SO_4. Subsequently, 160 µl of 0.5 µM malachite green in 0.1% (w/v) poly (vinyl alcohol) (PVA) were added, incubated for 30 min at room temperature. The absorption of the samples was detected at a wavelength of 620nm. The analyses were evaluated from at least three independent quadruplicate assays using GraphPad Prism 4 (GraphPad Software, USA).

4.2.6. TRANSFECTION

The open reading frame of full-length *Pf*ATC was cloned in front of the GFP gene of the expression vector pARL1a and was subsequently transfected into *P. falciparum* according to the protocol described in Chapter 3. Parasites were first observed after 16–60 days of selection and live parasites were analysed by fluorescent microscopy using an Axioskop 2 plus microscope (Zeiss). In order to visualize the nucleus, parasites were incubated with Hoechst 33342 dye according to the manufacturer's recommendation (Invitrogen). For colocalization experiments to visualize the endoplasmic reticulum, transfected *Plasmodium* was supplemented with 2 mM ER-Tracker Red BODIPY-TR (Invitrogen) prior to microscopy.

4.3. RESULTS

A truncated version of ATC from *P. falciparum* was cloned, recombinantly expressed, purified and crystallised. Full-length *Pf*ATC is a protein of 375 residues with a calculated molecular weight of 43.3 kDa. BLAST[38] analysis revealed no structural homologues for the first 36 N-terminal residues (Figure 4.3). *Pf*ATC shows 38% identity (84% query cover) to the catalytic subunit of ATC from *P. abyssi* (PDB entry 1ml4[30]; and 39% identity (84% query cover) to *E. coli* ATC (PDB entry 1d09[39]). Nucleotide BLAST analysis also shows 37% identity (86% query cover) to the ATC domain of human CAD (carbamoyl phosphate synthetase 2, aspartate transcarbamoylase and dihydroorotase) protein. The

crystal structure of this domain is not yet available, although preliminary data have been reported[40]. Further analysis with the PlasmoAP tool[41] showed a strong prediction for the N-terminal region to contain an apicoplast-targeting sequence, with a possible cleavage site between residues 27 and 28. GFP-labelling experiments *in vivo* showed distinct localization of *Pf*ATC compared with the endoplasmic reticulum, supporting the hypothesis of the apicomplexan nature of the enzyme (Figure 4.4). Based on these data, the third methionine in the sequence (Met37) was selected as the starting point of our construct.

Attempts to express and purify full-length *Pf*ATC with sufficient purity failed. SDS–PAGE analysis of the elution fraction of Strep-tag purification showed three distinct Strep-tagged (C-terminal) bands with sizes around 43kDa, and further size-exclusion purification showed three overlapping peaks that could not be separated with sufficient purity (data not shown). The use of protease-inhibitor cocktail during the lysis and purification did not show any significant improvement. The presence of at three versions of *Pf*ATC of different lengths in the elution fraction suggests that the full-length protein is proteolysed near the N-terminus owing to the apicoplast-targeting nature of this region. The activity assay performed with *Pf*ATC-Met3 showed that it possesses catalytic activity, and further experiments have been performed with this truncated *Pf*ATC construct. The recombinant *Pf*ATC was produced with a C-terminal Strep-tag (IBA Lifesciences) and was purified by Strep-tag chromatography according to the manufacturer's recommendations. In order to achieve higher purity and homogeneity, *Pf*ATC was further purified via SEC and the final product was assessed via SDS–PAGE analysis (Figure 4.1a). The yield of pure homogeneous protein was approximately 6 mg per litre of culture. In order to increase the post-purification stability of the protein sample and increase the chance of crystallisation, the SEC buffer was chosen based on the results of differential scanning fluorimetry. The freshly purified protein was concentrated to 9 mg ml^{-1} and used in protein crystallisation experiments. Multiple crystals of *Pf*ATC appeared overnight in various crystallisation screening conditions containing PEG (polyethylene glycol) 3350/4000. Optimization of the initial conditions yielded single *Pf*ATC crystals with a maximum dimension of 0.2 mm (Figure 4.1b). The optimized crystals diffracted X-rays to a maximum resolution of 2.4 Å on the ID23-2 beamline at ESRF, Grenoble, France. The space group of the *Pf*ATC crystals was determined to be monoclinic $P2_1$, with unit-cell parameters a = 87.0, b = 103.8, c = 87.1Å, α = 90.0, β = 117.7, γ = 90.0°. The presence of three *Pf*ATC molecules per asymmetric unit was confirmed by molecular replacement and the 2.5 Å resolution structure of *Pf*ATC has been deposited in the PDB with accession code 5ILQ.

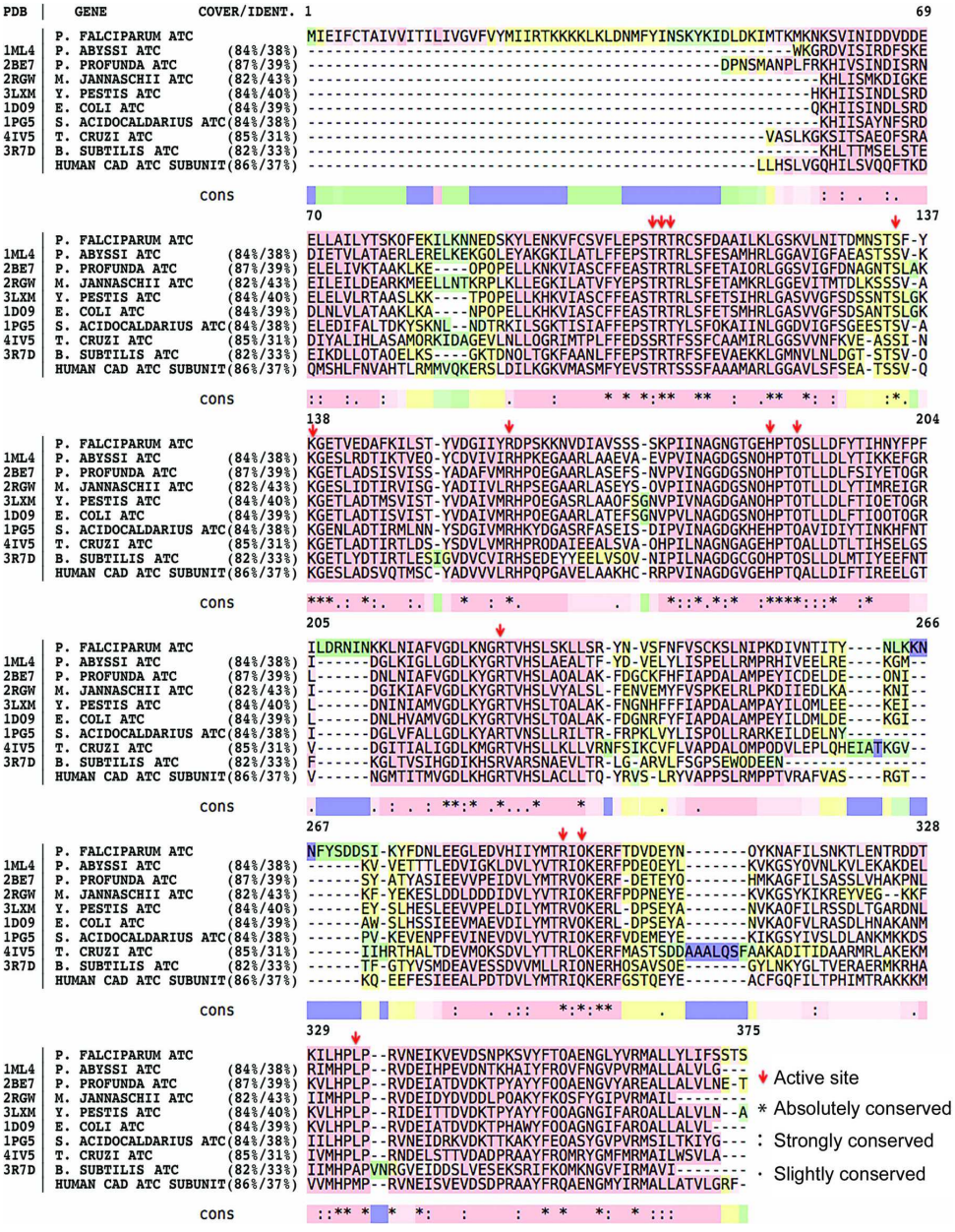

Figure 4.3 | The homology analysis of *Pf*ATC was performed using BLAST[38] and visualized via T-Coffee[42]. Red, yellow, green and blue colours represent good, average, bad and weak alignment, respectively. Residues essential for the active sites are shown with arrows. Absolutely, strongly and slightly conserved residues are marked with '*', ':' and '.' symbols, respectively.

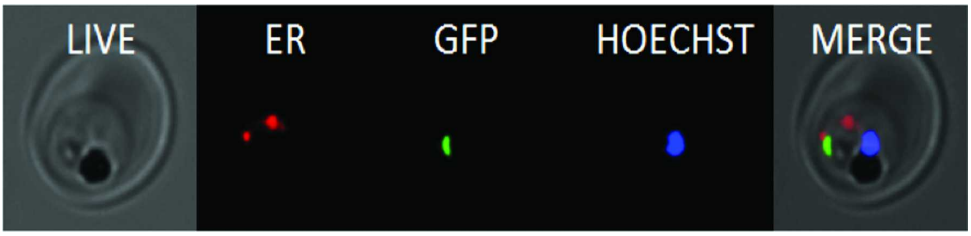

Figure 4.4 | Fluorescent microscopy imaging of *P. falciparum* transfected with GFP-labelled *Pf*ATC shows distinct localization of *Pf*ATC.

4.3.1. OVERALL STRUCTURE OF *Pf*ATC

*Pf*ATC is a homotrimer with three active sites formed across the oligomeric interfaces (Figure 4.5a). Superposition of the *Pf*ATC structure and the catalytic subunit of *E. coli* ATC (PDB entry 1d09[39]) showed a high level of sequence and secondary-structure conservation (Figure 4.3 and 4.6). BLAST analysis against nine known homologues (available structures) showed that of 375 residues, 46 (12.3%) were absolutely conserved, 43 (11.5%) were strongly conserved and 25 (6.7%) were slightly conserved. The loops formed by residues 84–91, 203–212 and 265–275 of *Pf*ATC are slightly longer than their *E. coli* analogues (residues 34–36, 150–155 and 206–208, respectively). In addition, the N-terminal region of the *Pf*ATC model (residues 37–48) is also longer and shows no secondary structure. Poor electron-density coverage suggests that this region is highly mobile. For this reason, the N-terminal residues 37–46 (chain A) and 37–43 (chains B and C) were excluded from the final model as well as the loops formed by residues 297–311 (all three chains) and the C-terminal region of chain A (residues 375–378). The presence of additional electron density near the C-terminus was modelled as the Strep-tag (SAWSHPQFEK) with the last 2–3 residues (FEK) excluded. All the active site residues of *Pf*ATC are conserved amongst the ATCs from other organisms (Figures 4.3 and 4.7) and each subunit of the trimer hosts an active site including two residues (Ser135 and Lys138) from the adjacent chain.

4.3.2. MUTAGENESIS STUDIES AND ACTIVITY PROFILE OF *Pf*ATC

Based on the mutagenic studies of *E. coli* ATC summarized in[46] and the overall structure similarity, a mutant *Pf*ATC version was generated. In *E. coli*, mutation of the essential active-site residues from the catalytic chain of ATC resulted in a significant loss of activity. For example, the guanidinium group of Arg54 of *E. coli* ATC was shown to be crucial for binding of the substrate carbamoyl phosphate (CP) and enzymatic condensation of CP and aspartate. Its removal (Arg54Ala mutation) caused a 17 000-fold

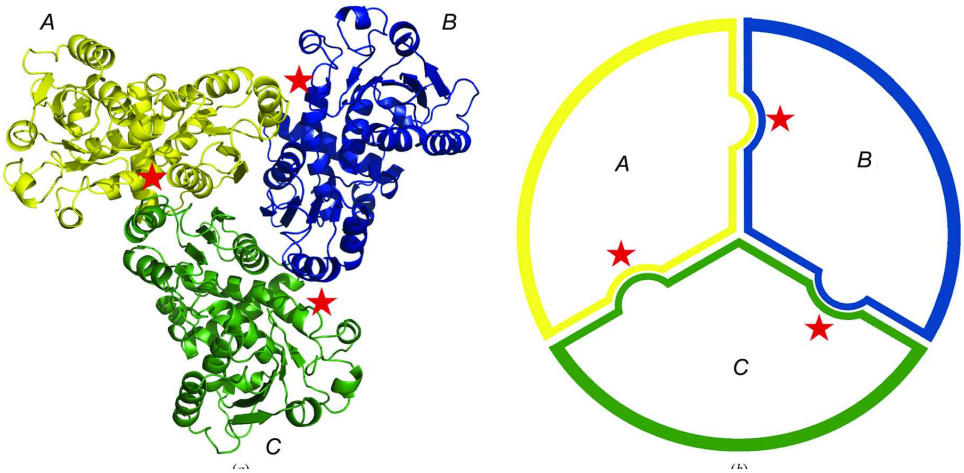

Figure 4.5 | The overall model of *Pf*ATC. (a) *Pf*ATC is a homotrimer with three active sites (shown with stars) formed at the oligomeric interfaces. (b) Schematic view of the *Pf*ATC homotrimer.

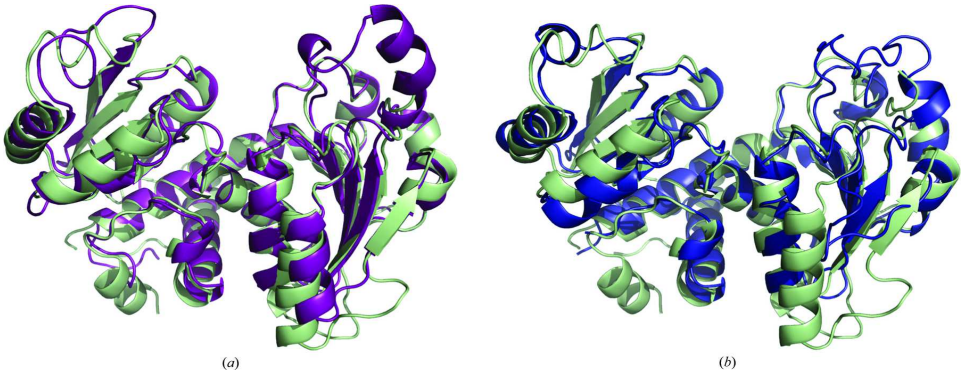

Figure 4.6 | The secondary structure of *Pf*ATC compared with *E. coli* ATC (a) and *B. subtilis* ATC (b). Coordinates of the *Pf*ATC structure (pale green) and the catalytic subunits of *E. coli* ATC in the liganded R state (magenta; PDB entry 1d09[39]) and of unliganded *B. subtilis* ATC (blue; PDB entry 3r7d[43] were superimposed using Coot[44]

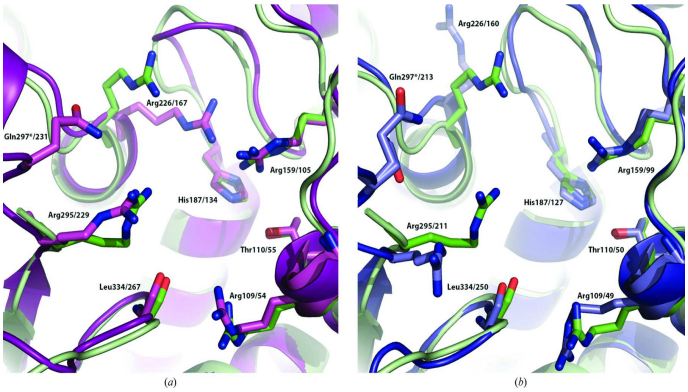

Figure 4.7 | PISA[45] analysis of the *Pf*ATC structure showed that the oligomeric contact between each pair of subunits (hereafter referred to as A and B) is formed by 32 residues [buried surface area (BSA) of 899 Å2] and 27 residues (BSA of 956 $Å^2$), respectively (Figure 4.8). The interface from the subunit A consists of nine absolutely conserved, three strongly conserved and two slightly conserved residues. The adjacent interface B has eight absolutely conserved, four strongly conserved and two slightly conserved residues. Each subunit has a total surface area of approximately 14 300 $Å^2$, of which 1855 $Å^2$ (13%) belongs to the intra-oligomeric interfaces.

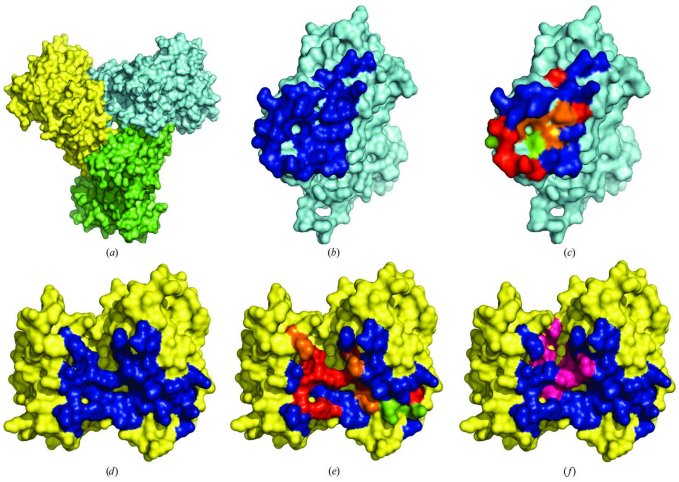

Figure 4.8 | PISA[45] analysis of the *Pf*ATC structure analysis reveals that each subunit forms two oligomeric contacts with other subunits of the trimer (a). The residues that form these contacts are shown in blue (b–f). Absolutely (red), strongly (orange) and slightly conserved (green) residues of these interfaces are shown (c, e). Active-site residues (magenta) are also shown on the surface (f).

loss in activity and a 13-fold reduction in the affinity for CP[47, 48]. The amino group of Lys84, which completes the active site of the adjacent subunit, interacts with both Arg54 and aspartate upon binding; a Lys84Asn mutation resulted in a 1200-fold activity loss for the *E. coli* enzyme[39]. Both mutations did not affect the folding and the structure of the enzyme, as confirmed by the X-ray data. Comparison between the crystal structures of *Pf*ATC and *E. coli* ATC (PDB entry 1d09[39]) showed that the Arg109 and Lys138 residues of the active site of *Pf*ATC are homologous to Arg54 and Lys84 of *E. coli* ATC. The mutant version *Pf*ATC-R109A/K138A was designed and cloned using the site-specific mutagenesis technique and was recombinantly expressed according to the same protocol as *Pf*ATC.

In order to confirm the presence of the catalytic activity of the recombinant *Pf*ATC, a phosphate-detection system based on malachite green[37] was established. The specific *in vitro* activity of *Pf*ATC was 11.04 ± 1.04 μmol min^{-1} mg^{-1}. Activity assays with the double mutant *Pf*ATC-R109A/K138A were also performed and showed a significantly lower value of 0.85 ± 0.30 μmol min^{-1} mg^{-1}.

4.4. DISCUSSION

The *de-novo* pyrimidine biosynthesis is a promising target pathway in antimalarial research[19] . The fourth enzyme of this pathway, dihydroorotate dehydrogenase (*Pf*DHODH), has been proposed as a potential drug target more than a decade ago[49] and first selective inhibitor, DSM1, was reported a few years later[50]. Multiple rounds of optimization led to the development of the compound DSM265, currently in clinical trials[51, 52]. The validation of DHODH demonstrates the potential of the plasmodial pyrimidine biosynthesis in the antimalarial drug discovery, suggesting that other enzymes within this pathway could also be explored as potential targets. The enzyme ATC is located upstream of DHODH[53, 54]. Here we reported the structure of *Pf*ATC, the localization of this enzyme within the malaria parasite and described the design of a mutant *Pf*ATC with significantly reduced catalytic activity.

The ATC from *Escherichia coli* was intensively studied, being a paradigm of feedback inhibition and a model of cooperativity and allosteric regulation[40, 46, 53–55]. It is important to remark that the basic catalytic conformation of this enzyme is composed of three subunits, possibly leading to the formation of a trimmer or a hexamer. This pattern is repeated in most of the species, including the here described, *Pf*ATC. Based on the structural information of *Pf*ATC and the mutagenic studies of *E. coli* ATC summarized in[46], we confirmed the initial hypothesis that mutation of the conserved active-site residues arginine 109 (R109A) and lysine 138 (K138A) would significantly reduce *Pf*ATC

catalytic activity. The possibility of adverse effect of these mutations on the folding or the oligomeric assembly of *Pf*ATC will be further discussed in Chapter 5. The analysis of the sequence and structure of *Pf*ATC revealed that the active site possesses high degree of conservation, making the structure-based design of specific active-site-targeting inhibitors of *Pf*ATC and further validation as a drug target highly challenging. On the other hand, the structure also revealed that, similar to what was observed for *E. coli* ATC, the active site of this enzyme is formed across the interface of two subunits and both polypeptide chains contribute to its binding pocket [46]. This feature would allow for assessment of essentiality of this enzyme via Protein Interference assay (PIA). Further experiments focused on this approach will be discussed in Chapter 5, in which complex formation between *Pf*ATC-WT and the R109A/K138A mutant *in vitro*, as well as transfection of *Pf*ATC-R109A/K138A to *P. falciparum*, are described.

REFERENCES

[1] M. J. Downie, K. Kirk, and C. B. Mamoun, *MINIREVIEWS Purine Salvage Pathways in the Intraerythrocytic Malaria Parasite,* Society **7**, 1231 (2008).

[2] M. B. Cassera, K. Z. Hazleton, E. F. Merino, N. Obaldia, M. C. Ho, A. S. Murkin, R. DePinto, J. A. Gutierrez, S. C. Almo, G. B. Evans, Y. S. Babu, and V. L. Schramm, *Plasmodium falciparum parasites are killed by a transition state analogue of purine nucleoside phosphorylase in a primate animal model,* PLoS One **6**, e26916 (2011).

[3] P. K. Rathod and P. Reyes, *Orotidylate-metabolizing enzymes of the human malarial parasite, plasmodium falciparum, differ from host cell enzymes,* Journal of Biological Chemistry **258**, 2852 (1983).

[4] P. Reyes, P. K. Rathod, D. J. Sanchez, J. E. K. Mrema, K. H. Rieckmann, and H.-g. Heidrich, *Enzymes of Purine and Pyrimidine Metabolism From the H U M a N,* Mol Biochem Parasitol **5**, 275 (1982).

[5] H. P. De Koning, D. J. Bridges, and R. J. S. Burchmore, *Purine and pyrimidine transport in pathogenic protozoa: From biology to therapy,* FEMS Microbiology Reviews **29**, 987 (2005).

[6] J. E. Hyde, *Drug-resistant malaria - an insight,* Febs J **274**, 4688 (2007).

[7] G. A. Kicska, P. C. Tyler, G. B. Evans, R. H. Furneaux, V. L. Schramm, and K. Kim, *Purine-less death in Plasmodium falciparum induced by immucillin-H, a transition*

state analogue of purine nucleoside phosphorylase, Journal of Biological Chemistry **277**, 3226 (2002).

[8] M. B. Cassera, K. Z. Hazleton, P. M. Riegelhaupt, E. F. Merino, M. Luo, M. H. Akabas, and V. L. Schramm, *Erythrocytic adenosine monophosphate as an alternative purine source in {Plasmodium} falciparum,* J Biol Chem **283**, 32889 (2008).

[9] W. Bungener and G. Nielsen, *Nucleic acid metabolism in experimental malaria. 1. Studies on the incorporation of thymidine, uridine, and adenosine in the malaria parasite (Plasmodium berghei and Plasmodium vinckei),* Z Tropenmed Parasitol **18**, 456 (1967).

[10] W. Büngener, *Incorporation of exogenous adenosine and hypoxanthine in the nucleic acids of malaria parasites (Plasmodium berghei and Plasmodium vinckei),* Zeitschrift fur Parasitenkunde (Berlin, Germany) **31**, 1 (1968).

[11] K. Van Dyke, G. C. Tremblay, C. H. Lantz, and C. Szustkiewicz, *The source of purines and pyrimidines in Plasmodium berghei.* The American journal of tropical medicine and hygiene **19**, 202 (1970).

[12] H. Polet and M. E. Conrad, *Malaria: Extracellular Amino Acid Requirements for in Vitro Growth of Erythrocytic Forms of Plasmodium knowlesi,* Experimental Biology and Medicine **127**, 251 (2013).

[13] C. J. WALSH and I. W. SHERMAN, *Purine and Pyrimidine Synthesis by the Avian Malaria Parasite, Plasmodium lophurae,* The Journal of Protozoology **15**, 763 (1968).

[14] S. M. TRACY and I. W. SHERMAN, *Purine Uptake and Utilization by the Avian Malaria Parasite Plasmodium lophurae,* The Journal of Protozoology **19**, 541 (1972).

[15] M. J. Gardner, N. Hall, E. Fung, O. White, M. Berriman, R. W. Hyman, J. M. Carlton, A. Pain, K. E. Nelson, S. Bowman, I. T. Paulsen, K. James, J. A. Eisen, K. Rutherford, S. L. Salzberg, A. Craig, S. Kyes, M. S. Chan, V. Nene, S. J. Shallom, B. Suh, J. Peterson, S. Angiuoli, M. Pertea, J. Allen, J. Selengut, D. Haft, M. W. Mather, A. B. Vaidya, D. M. Martin, A. H. Fairlamb, M. J. Fraunholz, D. S. Roos, S. A. Ralph, G. I. McFadden, L. M. Cummings, G. M. Subramanian, C. Mungall, J. C. Venter, D. J. Carucci, S. L. Hoffman, R. W. Davis, C. M. Fraser, and B. Barrell, *Genome sequence of the human malaria parasite Plasmodium falciparum,* Nature **419**, 498 (2002).

[16] M. A. Phillips and P. K. Rathod, *Plasmodium Dihydroorotate Dehydrogenase: A Promising Target for Novel Anti-Malarial Chemotherapy,* Infectious Disorders - Drug Targets **10**, 226 (2012), arXiv:NIHMS150003 .

[17] M. W. Mather, E. Darrouzet, M. Valkova-Valchanova, J. W. Cooley, M. T. McIntosht, F. Daldal, and A. B. Vaidya, *Uncovering the molecular mode of action of the antimalarial drug atovaquone using a bacterial system,* Journal of Biological Chemistry **280**, 27458 (2005).

[18] H. J. Painter, J. M. Morrisey, M. W. Mather, and A. B. Vaidya, *Specific role of mitochondrial electron transport in blood-stage Plasmodium falciparum.* Nature **446**, 88 (2007).

[19] A. B. Vaidya and M. W. Mather, *Mitochondrial Evolution and Functions in Malaria Parasites,* Annual Review of Microbiology **63**, 249 (2009).

[20] M. A. Phillips, K. L. White, S. Kokkonda, X. Deng, J. White, F. El Mazouni, K. Marsh, D. R. Tomchick, K. Manjalanagara, K. R. Rudra, G. Wirjanata, R. Noviyanti, R. N. Price, J. Marfurt, D. M. Shackleford, F. C. Chiu, M. Campbell, M. B. Jimenez-Diaz, S. F. Bazaga, I. Angulo-Barturen, M. S. Martinez, M. Lafuente-Monasterio, W. Kaminsky, K. Silue, A. M. Zeeman, C. Kocken, D. Leroy, B. Blasco, E. Rossignol, T. Rueckle, D. Matthews, J. N. Burrows, D. Waterson, M. J. Palmer, P. K. Rathod, and S. A. Charman, *A Triazolopyrimidine-Based Dihydroorotate Dehydrogenase Inhibitor with Improved Drug-like Properties for Treatment and Prevention of Malaria,* ACS Infectious Diseases **2**, 945 (2016).

[21] M. L. Booker, C. M. Bastos, M. L. Kramer, R. H. Barker, R. Skerlj, A. B. Sidhu, X. Deng, C. Celatka, J. F. Cortese, J. E. Guerrero Bravo, K. N. Crespo Llado, A. E. Serrano, I. Angulo-Barturen, M. B. Jiménez-Díaz, S. Viera, H. Garuti, S. Wittlin, P. Papastogiannidis, J. W. Lin, C. J. Janse, S. M. Khan, M. Duraisingh, B. Coleman, E. J. Goldsmith, M. A. Phillips, B. Munoz, D. F. Wirth, J. D. Klinger, R. Wiegand, and E. Sybertza, *Novel inhibitors of Plasmodium falciparum dihydroorotate dehydrogenase with antimalarial activity in the mouse model,* Journal of Biological Chemistry **285**, 33054 (2010).

[22] J. E. Nettleship, J. Brown, M. R. Groves, and A. Geerlof, *Methods for Protein Characterization by Mass Spectrometry, Thermal Shift (ThermoFluor) Assay, and Multiangle or Static Light Scattering,* (Humana Press, 2008) pp. 299–318.

[23] U. B. Ericsson, B. M. Hallberg, G. T. DeTitta, N. Dekker, and P. Nordlund, *Thermofluor-based high-throughput stability optimization of proteins for structural studies,* Analytical Biochemistry **357**, 289 (2006).

[24] U. K. Laemmli, *Cleavage of structural proteins during the assembly of the head of bacteriophage T4,* Nature **227**, 680 (1970), arXiv:arXiv:1011.1669v3 .

[25] A. N. Popov and G. P. Bourenkov, *Choice of data-collection parameters based on statistic modelling,* Acta Crystallographica - Section D Biological Crystallography **59**, 1145 (2003).

[26] M. Krug, M. S. Weiss, U. Heinemann, and U. Mueller, *XDSAPP : a graphical user interface for the convenient processing of diffraction data using XDS ,* Journal of Applied Crystallography **45**, 568 (2012).

[27] M. Diseases, *Solvent Content of Protein,* Journal of molecular biology **33**, 491 (1968).

[28] F. Long, A. A. Vagin, P. Young, and G. N. Murshudov, *BALBES: A molecular-replacement pipeline,* Acta Crystallographica Section D: Biological Crystallography **64**, 125 (2007).

[29] M. D. Winn, C. C. Ballard, K. D. Cowtan, E. J. Dodson, P. Emsley, P. R. Evans, R. M. Keegan, E. B. Krissinel, A. G. Leslie, A. McCoy, S. J. McNicholas, G. N. Murshudov, N. S. Pannu, E. A. Potterton, H. R. Powell, R. J. Read, A. Vagin, and K. S. Wilson, *Overview of the CCP4 suite and current developments,* Acta Crystallographica Section D: Biological Crystallography **67**, 235 (2011).

[30] S. Van Boxstael, R. Cunin, S. Khan, and D. Maes, *Aspartate transcarbamylase from the hyperthermophilic archaeon Pyrococcus abyssi: Thermostability and 1.8 Å resolution crystal structure of the catalytic subunit complexed with the bisubstrate analogue N-phosphonacetyl-L-aspartate,* Journal of Molecular Biology **326**, 203 (2003).

[31] P. Emsley, B. Lohkamp, W. G. Scott, and K. Cowtan, *Features and development of Coot ,* Acta Crystallographica Section D Biological Crystallography **66**, 486 (2010).

[32] G. N. Murshudov, A. A. Vagin, and E. J. Dodson, *Refinement of macromolecular structures by the maximum-likelihood method,* Acta Crystallographica Section D: Biological Crystallography **53**, 240 (1997).

[33] J. Painter and E. A. Merritt, *TLSMD web server for the generation of multi-group TLS models ,* Journal of Applied Crystallography **39**, 109 (2006).

[34] J. Painter and E. A. Merritt, *Optimal description of a protein structure in terms of multiple groups undergoing TLS motion,* Acta Crystallographica Section D: Biological Crystallography **62**, 439 (2006).

[35] W. L. Delano, *The PyMOL Molecular Graphics System,* (2002).

[36] I. B. Müller, J. Knöckel, M. L. Eschbach, B. Bergmann, R. D. Walter, and C. Wrenger, *Secretion of an acid phosphatase provides a possible mechanism to acquire host nutrients by {Plasmodium} falciparum,* Cellular Microbiology **12**, 677 (2010).

[37] S. Motomizu, T. Wakimoto, and Y. Tôei, *Determination of trace amounts of phosphate in river water by flow-injection analysis,* Talanta **30**, 333 (1983).

[38] S. F. Altschul, W. Gish, W. Miller, E. W. Myers, and D. J. Lipman, *Basic local alignment search tool,* Journal of Molecular Biology **215**, 403 (1990), arXiv:arXiv:1611.08307v1 .

[39] L. Jin, B. Stec, W. N. Lipscomb, and E. R. Kantrowitz, *Insights into the mechanisms of catalysis and heterotropic regulation of Escherichia coli aspartate transcarbamoylase based upon a structure of the enzyme complexed with the bisubstrate analogue N-phosphonacetyl-L-aspartate at 2.1 Å,* Proteins: Structure, Function and Genetics **37**, 729 (1999).

[40] A. Ruiz-Ramos, N. Lallous, A. Grande-García, and S. Ramón-Maiques, *Expression, purification, crystallization and preliminary X-ray diffraction analysis of the aspartate transcarbamoylase domain of human CAD,* Acta Crystallographica Section F: Structural Biology and Crystallization Communications **69**, 1425 (2013).

[41] B. J. Foth, S. A. Ralph, C. J. Tonkin, N. S. Struck, M. Fraunholz, D. S. Roos, A. F. Cowman, and G. I. McFadden, *Dissecting apicoplast targeting in the malaria parasite Plasmodium falciparum,* Science **299**, 705 (2003).

[42] P. Di Tommaso, S. Moretti, I. Xenarios, M. Orobitg, A. Montanyola, J. M. Chang, J. F. Taly, and C. Notredame, *T-Coffee: A web server for the multiple sequence alignment of protein and RNA sequences using structural information and homology extension,* Nucleic Acids Research **39**, W13 (2011).

[43] K. M. Harris, G. M. Cockrell, D. E. Puleo, and E. R. Kantrowitz, *Crystallographic snapshots of the complete catalytic cycle of the unregulated aspartate transcarbamoylase from Bacillus subtilis,* Journal of Molecular Biology **411**, 190 (2011).

[44] C. K., *Coot: model-building tools for molecular graphics. Acta Crystallogr., D,* Biol. Crystallogr. **60**, 2126 (2004).

[45] E. Krissinel and K. Henrick, *Inference of Macromolecular Assemblies from Crystalline State,* Journal of Molecular Biology **372**, 774 (2007).

[46] W. N. Lipscomb and E. R. Kantrowitz, *Structure and mechanisms of Escherichia coli,* Accounts of Chemical Research **45**, 444 (2012).

[47] J. W. Stebbins, D. E. Robertson, M. F. Roberts, R. C. Stevens, W. N. Lipscomb, and E. R. Kantrowitz, *Arginine 54 in the active site of {Escherichia} coli aspartate transcarbamoylase is critical for catalysis: a site-specific mutagenesis, {NMR}, and {X}-ray crystallographic study,* Protein Sci **1**, 1435 (1992).

[48] J. W. Stebbins, W. Xu, and E. R. Kantrowitz, *Three Residues Involved in Binding and Catalysis in the Carbamyl Phosphate Binding Site of Escherichia coli Aspartate Transcarbamylase,* Biochemistry **28**, 2592 (1989).

[49] J. E. Hyde, *Targeting purine and pyrimidine metabolism in human apicomplexan parasites.* Current drug targets **8**, 31 (2007).

[50] J. Baldwin, C. H. Michnoff, N. A. Malmquist, J. White, M. G. Roth, P. K. Rathod, and M. A. Phillips, *High-throughput screening for potent and selective inhibitors of Plasmodium falciparum dihydroorotate dehydrogenase,* Journal of Biological Chemistry **280**, 21847 (2005).

[51] K. A. Collins, T. Rückle, S. Elliott, L. Marquart, E. Ballard, S. Chalon, P. Griffin, J. J. Möhrle, and J. S. McCarthy, *DSM265 400 mg clears asexual stage parasites but not mature gametocytes from the blood of healthy subjects experimentally infected with Plasmodium falciparum ,* Antimicrobial Agents and Chemotherapy **63** (2019), 10.1128/aac.01837-18.

[52] J. M. Coteron, M. Marco, J. Esquivias, X. Deng, K. L. White, J. White, M. Koltun, F. El Mazouni, S. Kokkonda, K. Katneni, R. Bhamidipati, D. M. Shackleford, I. Angulo-Barturen, S. B. Ferrer, M. B. Jiménez-Díaz, F. J. Gamo, E. J. Goldsmith, W. N. Charman, I. Bathurst, D. Floyd, D. Matthews, J. N. Burrows, P. K. Rathod, S. A. Charman, and M. A. Phillips, *Structure-guided lead optimization of triazolopyrimidine-ring substituents identifies potent plasmodium falciparum dihydroorotate dehydrogenase inhibitors with clinical candidate potential,* Journal of Medicinal Chemistry **54**, 5540 (2011).

[53] A. Ruiz-Ramos, A. Velázquez-Campoy, A. Grande-García, M. Moreno-Morcillo, and S. Ramón-Maiques, *Structure and Functional Characterization of Human Aspartate Transcarbamoylase, the Target of the Anti-tumoral Drug PALA,* Structure **24**, 1081 (2016).

[54] J. M. West, H. Tsuruta, and E. R. Kantrowitz, *Stabilization of the R allosteric structure of Escherichia coli aspartate transcarbamoylase by disulfide bond formation,* Journal of Biological Chemistry **277**, 47300 (2002).

[55] G. M. Cockrell, Y. Zheng, W. Guo, A. W. Peterson, J. K. Truong, and E. R. Kantrowitz, *New paradigm for allosteric regulation of escherichia coli aspartate transcarbamoylase,* Biochemistry **52**, 8036 (2013).